Optics Letters

Optical generation and control of spatial Riemann waves

Domenico Bongiovanni,[1,2] Benjamin Wetzel,[1,3] Pengzhen Yang,[2] Yi Hu,[2,9] Yujie Qiu,[2] Jingjun Xu,[2] Stefan Wabnitz,[4,5] Zhigang Chen,[2,6,10] and Roberto Morandotti[1,7,8,11]

[1]INRS-EMT, 1650 Blvd. Lionel-Boulet, Varennes, Quebec J3X 1S2, Canada
[2]TEDA Applied Physics Institute and School of Physics, Nankai University, Tianjin 300457, China
[3]XLIM Research Institute, CNRS UMR 7252, Université de Limoges, 87060 Limoges, France
[4]DIET, Sapienza University of Rome, Via Eudossiana 18, 00184 Rome, Italy
[5]Novosibirsk State University, 1 Pirogova Street, 630090 Novosibirsk, Russia
[6]Department of Physics & Astronomy, San Francisco State University, San Francisco, California 94132, USA
[7]Institute of Fundamental and Frontier Sciences, University of Electronic Science and Technology of China, Chengdu 610054, China
[8]ITMO University, St. Petersburg 197101, Russia
[9]e-mail: yihu@nankai.edu.cn
[10]e-mail: zgchen@nankai.edu.cn
[11]e-mail: morandotti@emt.inrs.ca

Received 29 March 2019; revised 4 June 2019; accepted 12 June 2019; posted 17 June 2019 (Doc. ID 363703); published 11 July 2019

We extend the concept of Riemann waves (RWs) to the spatial domain and demonstrate for the first time, to the best of our knowledge, Riemann beams with a propagation scenario allowing controllable shock formation in a nonlinear optical system. Similar to their standard counterparts, "shifted" RWs are characterized by a local propagation speed proportional to their local amplitude. Their steepening dynamics can be judiciously controlled by means of an additional phase term. In particular, RWs are generated by properly tailoring the initial phase of an optical beam propagating through a thermal solution of an m-cresol/nylon mixture that exhibits a giant self-defocusing nonlinearity. The experimental results show a controllable steepening and shock wave behavior, in good agreement with the prediction from the simple inviscid Burgers equation.

https://doi.org/10.1364/OL.44.003542

For over a decade, nonlinear optics has provided a convenient and controllable environment to investigate nontrivial wave phenomena and establish intriguing links with those encountered in hydrodynamics [1]. The analogy arises from the central role of the nonlinear Schrödinger equation (NLSE) that may describe both optical and hydrodynamic nonlinear systems. Stimulated by the seminal observation of "optical rogue waves," [2] research in this field has led to several studies in optics, with the aim of studying the origin and the control of extreme event formation [3–6]. In this framework, the self-focusing regime of the NLSE and its similarity with deep-water wave hydrodynamics [7,8] have received significant attention, in particular within optical studies focusing on the process of modulation instability [1,9–11] and the associated formation of peculiar nonlinear solutions (such as optical breathers and solitons) [1]. Remarkably, the self-defocusing regime of the NLSE can also exhibit ubiquitous phenomena found in a broad range of physical systems, well beyond nonlinear optics. For instance, besides the well-known optical dark solitons [12], the self-defocusing NLSE, upon particular assumptions, can efficiently mimic the dynamics of shallow water hydrodynamics [13,14]. In particular, whenever nonlinearity is predominant over a linear beam or pulse broadening [15–17], the NLSE can be approximated into the nonlinear shallow water equation (NSWE), the study of which has been the focus of several recent works. Noteworthy, this NSWE analogy in nonlinear optics has been at the basis of studies spanning the formation of optical undular bores [18], optical tsunamis [19], hydrodynamic optical soliton tunneling [20], and the experimental study of photonic dam breaks [21]. The underlying interest in the NSWE approximation comes from the availability of several analytic solutions that can be readily calculated [15]. For instance, nonlinear invariant solutions of the NSWE, also known as Riemann waves (RWs) [19,22], are of particular significance for their intrinsic relation with shock wave phenomena [23–29]. Perhaps the most exemplary among recent works are the observation of random RW signatures in integrable turbulences [30] and the controlled excitation of "simple" RWs [31] in nonlinear optical fibers. The temporal evolution of the RW is known to obey the inviscid Burgers equation (IBE) [15] —a ubiquitous and simple model used to study shock wave formation in different areas of physics [32–34], from traffic flow [35] to optical tsunamis [19].

In this Letter, we experimentally study simple RWs in the spatial domain, extending the spatial analogy to shifted Riemann beams (RBs). Guided by our theoretical analysis, we demonstrate experimentally the formation of optical RBs by judiciously shaping a laser beam before entering into a synthetic

colloidal suspension. Specifically, we show that the transverse position of the shock point can be tailored by means of a linear phase shift. We observed such shifted RBs in m-cresol/nylon thermal solutions, which provide the sufficient self-defocusing nonlinearity [36] required to approximate the spatial beam evolution by the NSWE.

To theoretically describe our approach, we start by approximating the response of our thermal solution with an instantaneous Kerr nonlinearity (see, e.g., [36]), where the beam evolution is described by the following one-dimensional (1D) NLSE:

$$i\frac{\partial E}{\partial z}+\frac{1}{2k}\frac{\partial^2 E}{\partial x^2}+\gamma|E|^2E=0. \tag{1}$$

In Eq. (1), $E(x,z)$ is the electric field envelope, $\gamma=kn_2/n_0$ is the nonlinear coefficient, and $k=k_0n_0$ is the wavenumber, in which n_0 is the refractive index, k_0 is the vacuum wave vector, and n_2 is the second-order nonlinear refractive index. In a dimensionless coordinate system, Eq. (1) can be rewritten as

$$i\frac{\partial \psi}{\partial \xi}+\frac{1}{2}\frac{L_{\mathrm{NL}}}{L_{\mathrm{Diff}}}\frac{\partial^2\psi}{\partial s^2}+\mathrm{sgn}(\gamma)|\psi|^2\psi=0, \tag{2}$$

where $s=x/x_0$ and $\xi=z/(\gamma I_0)$ correspond to the dimensionless transverse and longitudinal coordinates, scaled with respect to the beam waist x_0 and the peak intensity I_0; $\psi(s,\xi)=E(s,\xi)/I_0^{1/2}$ is the normalized electric field envelope, while $L_{\mathrm{NL}}=1/(|n_2|I_0)$ and $L_{\mathrm{Diff}}=1/(k_0n_0x_0^2)$ refer to the nonlinear and diffraction lengths, respectively. The solutions to Eq. (2) are found by applying the Madelung-like transformation [16]

$$\psi(s,\xi)=\sqrt{\rho(s,\xi)}\,\exp\left[\pm i\sqrt{\frac{L_{\mathrm{Diff}}}{L_{\mathrm{NL}}}}\int_{-\infty}^{s}u(s',\xi)\mathrm{d}s'+i\alpha s\right], \tag{3}$$

where $\rho(s,\xi)$ and $u(s,\xi)$ are real functions, and α corresponds to a linear phase-shift parameter. If we consider a strongly self-defocusing nonlinear regime (so that $n_2<0$, and $L_{\mathrm{Diff}}\gg L_{\mathrm{NL}}$), Eq. (2) can be approximately described by the following NSWE:

$$\begin{aligned}&\frac{\partial\rho}{\partial\varsigma}+(u\pm a\beta)\frac{\partial\rho}{\partial s}+\rho\frac{\partial u}{\partial s}=0\\&\frac{\partial u}{\partial\varsigma}+\frac{\partial\rho}{\partial s}+(u\pm a\beta)\frac{\partial u}{\partial s}=0,\end{aligned} \tag{4}$$

with $\beta=(L_{\mathrm{NL}}/L_{\mathrm{Diff}})^{1/2}$ and $\varsigma=\beta\xi$. Within this regime, we can further assume that the input excitation has the form of a simple RW [22] (denoted with $\psi R(s,\xi)$), a solution that complies with the relationship $u(s,\xi)=2[\rho(s,\xi)]^{1/2}$. In this particular case, the instantaneous spatial frequency profile of the beam is a scaled replica of its amplitude. More importantly, during nonlinear propagation, the beam tends to preserve this proportionality between spatial chirp and amplitude; thus, the beam dynamics, formally governed by the NLSE, can now be efficiently approximated by the IBE:

$$\frac{\partial|\psi_R|}{\partial\xi}\pm(3\beta|\psi_R|\pm\alpha\beta^2)\frac{\partial|\psi_R|}{\partial s}=0. \tag{5}$$

The above equation can be analytically solved through the method of characteristics, which indicates the direction of the energy flow in the RW. In its implicit form, the solution can be expressed as

$$|\psi_R(s,\xi)|=|\psi_R(s-\alpha\beta^2\xi\mp3\xi\beta|\psi_R(s,\xi)|)|, \tag{6}$$

while the characteristic lines are described by the parametric representation

$$s(s_0,\xi)=s_0+\alpha\beta^2\xi\pm3\xi\beta|\psi_R(s_0,0)|, \tag{7}$$

where s_0 denotes an arbitrary point in the s-axis at the onset of propagation (i.e., $\xi=0$). Depending on the sign in Eq. (3), which also governs the signs in Eqs. (4)–(7), the IBE solution is associated with a progressive steepening of either its left or right edge, along with the eventual development of a gradient catastrophe associated with the formation of a shock. At the shock point (s_{SC}, ξ_{SC}), the characteristic lines start to cross in the s-ξ plane, so that the wave amplitude derivative tends to go to infinity. In fact, this point can be readily calculated as $s_{SC}=s_{0SC}+\alpha\beta^2\xi_{SC}\pm3\xi_{SC}\beta|\psi_R(s_{0SC},0)|$ and $\xi_{SC}=(-3\beta\partial|\psi_R(s_{0SC},0)|/\partial s)^{-1}$, with s_{0SC} being the value corresponding to $\min[(-\partial|\psi_R(s,0)|/\partial s)^{-1}]$.

According to the above theory, we expect that the inclusion of a linear phase-shift α will allow for the direct control of the RW transverse shock position s_{SC}, while the distance ξ_{SC} at which this shock develops is expected to remain unchanged. (Note that the case where $\alpha=0$ here corresponds to the standard, simple RW reported in the literature [19,22,31].) Numerically, we study the evolution of this solution within the framework of the (1D) spatial NLSE. In particular, we consider the case of shifted RBs described by Eq. (3), where the input beam presents a Gaussian shape. Figure 1 reports numerical simulations for the case of a Gaussian RB propagating in a 2 cm long nonlinear medium, with parameters $\beta=0.035$ and $\gamma=-3.86\times10^{-5}$ mW^{-1} (so that the NLSE can be effectively approximated by the NSWE). The simulations are carried out via the split-step Fourier transform method applied to Eq. (1).

At the input, we consider a RB with an amplitude profile $E(x,0)=I_0^{1/2}\exp(x^2/2x_0^2)$, with $x_0=169$ μm and $I_0=81.9$ kW/m^2. We assume the sign of the spatial chirp in Eq. (3) to be positive, and consider two different values of the shifting parameter $\alpha=-6\times10^5$ and 0. For the first negative value of α, the Gaussian RB conserves a constant peak intensity while moving backward along the x-axis, as illustrated in Figs. 1(a) and 1(b). Simultaneously, the beam undergoes a progressive steepening of its right edge until reaching a near-infinity slope at the shock point, the position of which is given by $z_{SC}=e^{1/2}/(3\beta\gamma I_0)=10$ mm and $x_{SC}=2x_0+e^{1/2}x_0^2\alpha\beta/3=6.1$ μm. In this case, with the inclusion of an additional phase shift leading to a tilt of the beam front, the low-intensity parts of the beam travel faster towards the left than the high-intensity ones. Conversely, for the case illustrated in Figs. 1(c) and 1(d) where $\alpha=0$ (as well as for other positive values of α), the RB shifts forward along the x-axis, while experiencing a similar steepening behavior until the formation of the gradient catastrophe (shock) is reached at $z_{SC}=10$ mm and $x_{SC}=0.34$ mm. Without the beam front tilt induced by the additional phase term α, RB propagation is similar to the case of a standard RW, theoretically studied in Refs. [19,22], where the high-intensity parts of the beam travel faster towards the right than the low-intensity ones. The qualitatively different behavior observed in the NLSE simulations, including the beam front tilt, is indeed confirmed by the analysis of the characteristic lines obtained from Eq. (7) and depicted with

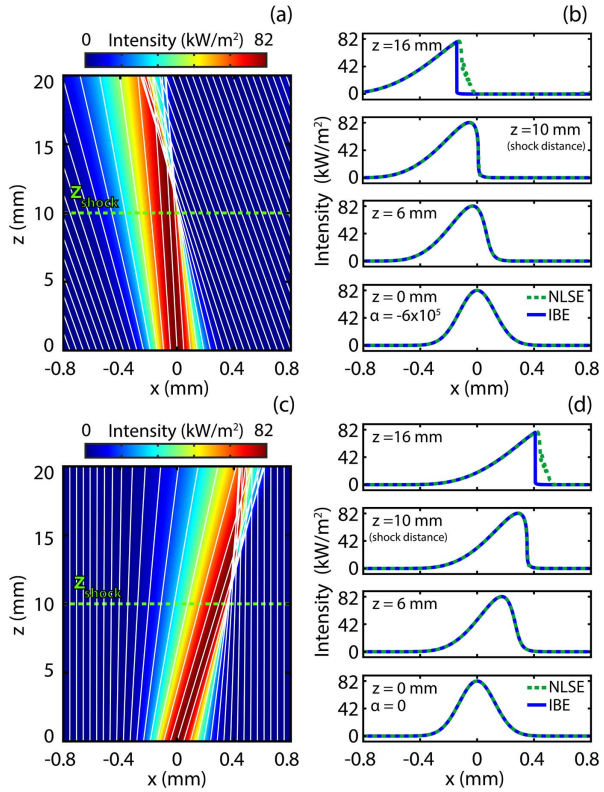

Fig. 1. Numerical demonstration of RB propagation obtained for two different values of the linear shift parameter, exhibiting the shock formation at the same distance $z = 10$ mm. The parameters in the NLSE simulations are $\beta = 0.035$ and $\gamma = -3.86 \times 10^{-5}$ mW^{-1}. (a), (b) $\alpha = -6 \times 10^5$ and (c), (d) $\alpha = 0$. The simulated beam intensity evolutions (a), (c) are compared with the characteristic lines obtained analytically from the IBE predictions (white lines). The corresponding intensity profiles (b), (d) at selected distances compare the NLSE simulations (dashed green) with the IBE evolutions (solid blue).

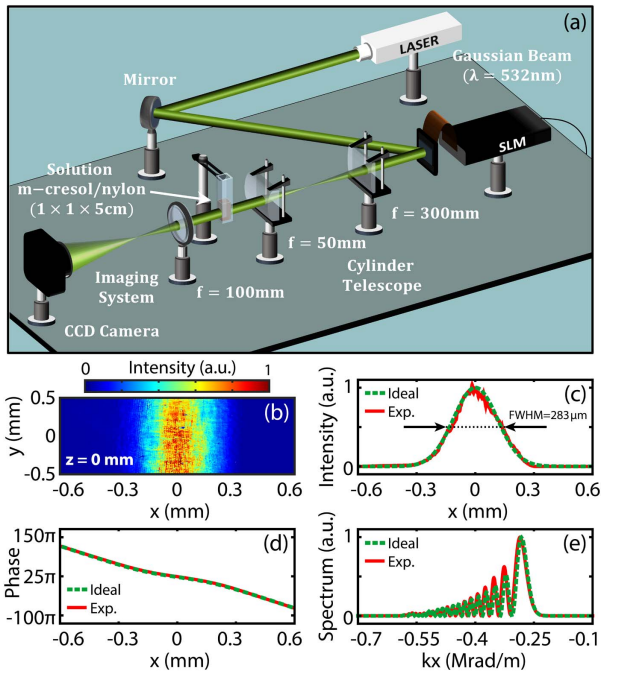

Fig. 2. (a) Experimental setup. (b) Transverse intensity distribution of the RB measured at the input facet of the cuvette. (c) Mean intensity profile (solid red line) corresponding to (b) and its Gaussian fit (dashed green line). (d) Input spatial phase and (e) spectral intensity profiles are calculated using either the ideal Gaussian fit (dashed green line) or the real experimental conditions (solid red line) shown in (c).

white lines in Figs. 1(a) and 1(c): until the shock distance z_{SC} (after which the IBE solution is no longer valid), the numerical evolution of the NLSE is in very good agreement with the IBE analytical predictions, as also attested by the perfect overlap between the selected intensity profiles illustrated in Figs. 1(b) and 1(d).

Shifted RWs represent a more general class of simple invariant solutions of the NSWE system, which we aim at observing experimentally using the setup of Fig. 2(a). In contrast with Ref. [31], where temporal RWs (i.e., pulses) were generated by shaping both amplitude and phase in the Fourier domain, spatial RWs (i.e., RBs) are synthesized by solely modulating the input beam phase in the real space. The phase of an incident Gaussian beam (continuous wave, $\lambda = 532$ nm, 1.4 mm waist) is shaped via a commercial phase-only spatial light modulator (SLM) produced by Holoeye (Pluto −1920 × 1080 pixels). A cylindrical telescope system ($f = 300$ mm and $f = 50$ mm) is employed to reshape the phase-modulated circular Gaussian beam into an elliptical one (FWHM = 283 μm along the minor axis and 2.31 mm along the major axis; 58 mW). The cylinder telescope here possesses a dual-functionality: First, it allows to approximate the experimental conditions of the 1D NLSE (by making the beam quasi-invariant along the y-axis); secondly, it enables to properly scale the applied phase mask (and beam intensity) in order to generate the desired input conditions, while fully exploiting the spatial resolution and power limitations of the SLM. After its initial shaping, the RB is injected into a 1 cm long cuvette filled with a nonlinear thermal solution composed of an m-cresol and nylon mixture. For 3.5% mass concentration of nylon, the nonlinear Kerr coefficient associated with the solution is estimated to be $n_2 = -1.6 \times 10^{-5}$ cm^2/W [36]. The strong nonlinearity of this solution, along with the beam parameters, allows us to reach NSWE validity for the NLSE system ($\beta \approx 0.035$). The beam characterization is carried out by recording the transverse intensity distributions at the front and back facets of the cuvette using a spherical lens ($f = 100$ mm) and a CCD camera (Coherent LaserCam-HR II).

First, we measured the intensity pattern of the initial laser beam at the input facet. This "noisy" 2D beam intensity pattern shown in Fig. 2(b) was then averaged along the y-axis, in order to retrieve a 1D beam intensity profile [see Fig. 2(c)], which was used to compute the appropriate RB phase mask. As mentioned above, simple RBs exhibit a spatial chirp that is a properly scaled replica of their amplitude. In this case, the experimental intensity profile (solid red line) was well fitted by a Gaussian profile (dashed green line), similarly to the simulations reported in Fig. 1. To imprint the appropriate spatial chirp, the phase information for SLM encoding was numerically calculated using Eq. (3), and considering the fitted intensity profile shown in Fig. 2(c): With a linear phase shift $\alpha = -6 \times 10^5$, the overall horizontal phase mask shown in Fig. 2(d) leads to the formation of a RB with a highly modulated input spectrum [Fig. 2(e)], where the experimental

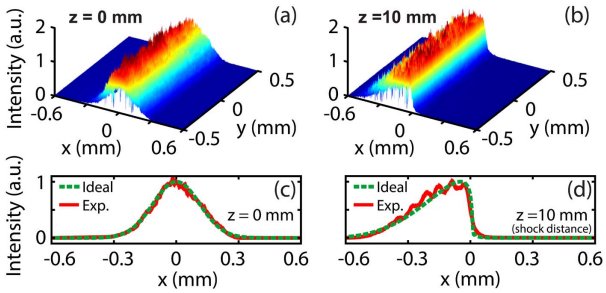

Fig. 3. Three-dimensional plot of (a), (b) intensity distributions and (c), (d) corresponding intensity profiles of the 1D RB at the (a), (c) input and (b), (d) output of a 1 cm long cuvette filled with a nonlinear thermal solution. (a), (b) Experimental measurements. (c), (d) Comparison of the intensity profiles obtained experimentally (solid red) and IBE predictions (dashed green).

profile (solid red line) is in good agreement with the numerically calculated one (dashed green line). Experimentally, we characterized the input intensity pattern at a low power level (∼1 mW), for which it was confirmed that any nonlinear beam reshaping was absent after propagation. However, at a target power level (58 mW), the laser beam experienced a strong nonlinear self-defocusing effect, thus activating the controlled steepening of the RB. We mention that the linear loss (measured to be 0.2 cm^{-1}) in our defocusing media is not negligible, but plays a minor role during the evolution of the RB.

Figure 3 compares the numerical and experimental results of a spatial RW dynamics signature. The input beam [Figs. 3(a) and 3(c)] experiences progressive steepening, until a vertical edge is formed at the output [Figs. 3(b) and 3(d)], after 1 cm of propagation in the solution. The experimental intensity patterns shown in Figs. 3(a) and 3(b) are in good quantitative agreement with numerically simulated dynamics: the averaged intensity profiles displayed in Figs. 3(c) and 3(d) highlight how the experimentally observed RB steepening process (red lines) leads to the formation of a shock at the foreseen propagation distance $z_{SC} = 1$ cm, in good agreement with IBE predictions (green lines). It is noteworthy that the shifted RB is here efficiently engineered, so that the shock formation occurs at the beam center (i.e., the steepened edge is located at $x_{SC} = 0$) without the appearance of the post-shock oscillations typically observed on a non-zero intensity background [22,27,29,31]. Conversely, some oscillations are observed on the RB left edge, mainly due to imperfect spectral filtering of the high-order diffractive terms introduced by the SLM, as well as to the scattering effects induced by the nylon particles dissolved in the m-cresol solvent.

In conclusion, we have introduced a new, and more general class of spatial optical RW solutions. Taking advantage of the giant self-defocusing nonlinearity offered by synthetic m-cresol/nylon thermal solutions, shifted RBs are observed experimentally via spatial shaping, providing a good qualitative agreement with the IBE theoretical predictions of shock formation. The ability to generate these ubiquitous wave dynamics in the spatial domain (where the evolution is not limited to one dimension [27–32]) offers new perspectives to exploit advanced and controllable high-dimensional RW dynamics.

Funding. Natural Sciences and Engineering Research Council of Canada (NSERC); Ministère de l'Économie, de la Science et de l'Innovation—Québec (MESI); Key Programme (2017YFA0303800); National Natural Science Foundation of China (NSFC) (61575098, 91750204); Plasma Québec; Ministry of Education and Science of the Russian Federation (Minobrnauka) (14.Y26.31.0017); ITMO Fellowship and Professorship Program (074-U01); 1000 Talents Sichuan Program.

REFERENCES

1. J. M. Dudley, F. Dias, M. Erkintalo, and G. Genty, Nat. Photonics **8**, 755 (2014).
2. D. R. Solli, C. Ropers, P. Koonath, and B. Jalali, Nature **450**, 1054 (2007).
3. D. R. Solli, C. Ropers, and B. Jalali, Phys. Rev. Lett. **101**, 233902 (2008).
4. J. M. Dudley, G. Genty, and B. J. Eggleton, Opt. Express **16**, 3644 (2008).
5. B. Wetzel, A. Stefani, L. Larger, P. A. Lacourt, J. M. Merolla, T. Sylvestre, A. Kudlinski, A. Mussot, G. Genty, F. Dias, and J. M. Dudley, Sci. Rep. **2**, 882 (2012).
6. Z. Yang, W. P. Zhong, M. Belić, and Y. Zhang, Opt. Express **26**, 7587 (2018).
7. T. B. Benjamin and J. E. Feir, J. Fluid Mech. **27**, 417 (1967).
8. N. Akhmediev and E. Pelinovsky, Eur. Phys. J. Spec. Top. **185**, 1 (2010).
9. M. Erkintalo, K. Hammani, B. Kibler, C. Finot, N. Akhmediev, J. M. Dudley, and G. Genty, Phys. Rev. Lett. **107**, 253901 (2011).
10. D. R. Solli, G. Herink, B. Jalali, and C. Ropers, Nat. Photonics **6**, 463 (2012).
11. J. M. Soto-Crespo, A. Ankiewicz, N. Devine, and N. Akhmediev, J. Opt. Soc. Am. B **29**, 1930 (2012).
12. Y. S. Kivshar and B. Luther-Davies, Phys. Rep. **298**, 81 (1998).
13. B. Varlot, S. Wabnitz, J. Fatome, G. Millot, and C. Finot, Opt. Lett. **38**, 3899 (2013).
14. S. Wabnitz, C. Finot, J. Fatome, and G. Millot, Phys. Lett. A **377**, 932 (2013).
15. G. B. Whitham, *Linear and Nonlinear Waves* (Wiley, 1974).
16. Y. Kodama and S. Wabnitz, Opt. Lett. **20**, 2291 (1995).
17. Y. Kodama, SIAM J. Appl. Math. **59**, 2162 (1999).
18. J. Fatome, C. Finot, G. Millot, A. Armaroli, and S. Trillo, Phys. Rev. X **4**, 021022 (2014).
19. S. Wabnitz, J. Opt. **15**, 064002 (2013).
20. P. Sprenger, M. A. Hoefer, and G. A. El, Phys. Rev. E **97**, 032218 (2018).
21. G. Xu, M. Conforti, A. Kudlinski, A. Mussot, and S. Trillo, Phys. Rev. Lett. **118**, 254101 (2017).
22. S. Malaguti, A. Corli, and S. Trillo, Opt. Lett. **35**, 4217 (2010).
23. V. Gurevich, A. L. Krylov, and G. A. El, Sov. Phys. JETP **74**, 957 (1992).
24. L. Francarollo and H. Capart, J. Fluid Mech. **461**, 183 (2002).
25. N. Zahibo, E. Pelinovsky, T. Tapilova, and I. Nikolkina, J. Geophys. Res. **115**, B03402 (2010).
26. A. Didenkulova and E. Pelinovsky, Nonlinearity **24**, R1 (2011).
27. S. Trillo and M. Conforti, in *Handbook of Optical Fibers*, G.-D. Peng, ed. (Springer, 2017), pp. 1–48.
28. W. Wan, S. Jia, and J. W. Fleisher, Nat. Phys. **3**, 46 (2007).
29. G. Xu, D. Vocke, D. Faccio, J. Garnier, T. Roger, S. Trillo, and A. Picozzi, Nat. Commun. **6**, 8131 (2015).
30. S. Randoux, F. Gustave, P. Suret, and G. El, Phys. Rev. Lett. **118**, 233901 (2017).
31. B. Wetzel, D. Bongiovanni, M. Kues, Y. Hu, Z. Chen, S. Trillo, J. M. Dudley, S. Wabnitz, and R. Morandotti, Phys. Rev. Lett. **117**, 073902 (2016).
32. Y. B. Zel'Dovich, Astron. Astrophys. **5**, 84 (1970).
33. J. L. Hammack and H. Segur, J. Fluid Mech. **65**, 289 (1974).
34. J. Bec and K. Khanin, Phys. Rep. **447**, 1 (2007).
35. D. Chowdhury, L. Santen, and A. Schadschneider, Phys. Rep. **329**, 199 (2000).
36. V. Smith, B. Leung, P. Cala, Z. Chen, and W. Man, Opt. Mater. Express **4**, 1807 (2014).